Available online at www.sciencedirect.com
SCIENCE DIRECT®

Journal of the European Ceramic Society 23 (2003) 1477–1484
www.elsevier.com/locate/jeurceramsoc

The influence of oxidation on crack resistance in injection moulded Cr_3C_2/Al_2O_3 composites

Ching-An Jeng, Jow-Lay Huang*

Deparment of Material Science and Engineering, National Cheng-Kung University, Tainan, 701 Taiwan, ROC

Received 20 June 2002; received in revised form 12 September 2002; accepted 22 September 2002

Abstract

The crack resistance (R-curve) of injection moulded Cr_3C_2/Al_2O_3 composite was studied using the indentation-strength-in-bending technique. The influence of heat treatment on the crack resistance was investigated. The oxidation layer containing alumina and alumina/chromia solid solution was in a compression of −179 and −195 MPa as evaluated by X-ray analysis and indentation method, respectively. The results were slightly different from the thermal mismatch calculation (−139 MPa). The relatively compressive, low porous oxidation layer caused significant increase in crack resistance. Crack healing could contribute also partially to crack resistance.

Keywords: Al_2O_3; Composite; Crack resistance; Cr_3C_2/Al_2O_3; Oxidation; Residual stress

1. Introduction

Improvement in fracture resistance of ceramic materials has been achieved by dispersing secondary metals or ceramic phases. Chromium carbide has been proved to be a potential material for toughening alumina because of its high Young's modulus and erosion resistance.[1] Promising mechanical properties and high temperature oxidation resistance of Cr_3C_2/Al_2O_3 composites were formerly reported by Fu et al.[2,3] It was previously reported that Cr_3C_2 was relatively stable under low equilibrium oxygen pressure and had a tendency to convert into Cr_7C_3 with increase in temperature.[3–6] It was formerly discussed that the room temperature strength and toughness of Cr_3C_2 particle-reinforced Al_2O_3 composites could be improved through the oxidation treatment.[3] However, the effect of oxidation on fracture behavior and the role of residual stress remain unclear.

Some effective methods for introducing a beneficial macroscopic compressive stress for improving mechanical properties have been tried. Strengthening glass-ceramics by compressive glazes and strength improvement in alumina–zirconia composites by transformation-induced stresses are typical examples.[7–10] The introduction of residual compressive surface stress was found to suppress substantially cracking during the loading cycle in glass indentation fracture.[11]

Most of the previous research on oxidation effects has concentrated on the bending strength, fracture toughness and reliability.[2,12–14] More recently, Damani and Lutz observed that annealed plasma-sprayed alumina exhibited pronounced R-curve behavior.[15] Few studies have been performed on the oxidation of composites which pertain directly to crack resistance (R-curve) behavior. The objective of this study was to investigate the influence of oxidation on the crack resistance of Cr_3C_2/Al_2O_3 composites. The injection molding technique was used to fabricate complex-shaped components of high-dimensional accuracy with potential for automatic production.

2. Experimental procedure

2.1. Material preparation

Alumina powders (A16-SG, Alcoa, USA 0.5 μm) were mixed with Cr_3C_2 (2 μm, grade 160, H.C Stark,

* Corresponding author. Fax: +886-6-276-3586.
E-mail address: JLH888@mail.ncku.edu.tw (J.-L. Huang).

0955-2219/03/$ - see front matter © 2003 Elsevier Science Ltd. All rights reserved.
doi:10.1016/S0955-2219(02)00363-1

Goslar, Germany. 10 vol.%) in a polyurethane bottle with high purity alumina balls and ethanol for 24 h. The slurry was dried in a rotating vacuum evaporator for 20 min. Dried agglomerates were ground with an alumina mortar and pestle, and screened through a 100 mesh screen to remove aggregates. The above powders were first mixed in a sigma blender (Irie Shokai Co., Japan, PN-1H) for 40 min. The binders (44 vol.%) were subsequently added and mixed for another 40 min. The temperature of the mixer was maintained at 200 °C by hot circulating oil. The binder system contained polypropylene (UBE Indu. Ltd., Japan), paraffin wax (Fluka, Japan) and stearic acid (Katayama, Japan) at a weight ratio of 30:65:5.

Green compacts with dimensions of 65×6.1×5.1 mm were molded using a reciprocating screw injection molding machine (Chen Hsong Machinery Taiwan Co. Ltd., SM-50) under a pressure of 70 MPa, with a holding time of 8 s and injecting velocity of 40 cc/s. The barrel temperatures used for injection were 150, 155, 160, 165 °C from feeder to nozzle. Test samples were soaked in heptane at 40 °C for 5 h, dried in ambient air, and thermally debinded. Samples were then cold isostatically pressed at 100 MPa and sintered in a graphite furnace at 1550 °C for 2 h under vacuum. They were then ground, lapped (GC#600) and polished to 1μm finish. The samples were oxidized in a molydisilicide-heated furnace in air at temperatures up to 1200 °C for 36 h before test.

2.2. Evaluation of physical and mechanical properties

The density was measured by the Archimedes method and the hardness was determined by a microhardness indentor (Vickers, Hv. Akashi AVK-A, Japan). The elastic modulus and Poisson's ratio were evaluated by pulse echo method (pulse generator, model 5072, Panametrics, USA and oscilloscope, TDS540C, Tektronix, USA). The thermal expansion coefficients were measured by a self-designed dilatometry system. Flexural strength of samples were measured by four-point bending test on a universal testing instrument (Series 8562, Instron Corporation. Canton MA, USA) at a displacement rate of 0.5 mm/min. The outer and inner spans were 40 and 20 mm respectively. Testing samples were machined into bars with dimensions of 4×5×50 mm with 45° edge chamfers. Each of the data points reported represents the average of more than seven tests.

2.3. Microstructural analysis and stress measurement

Microstructure and fractured surfaces were examined by optical microscopy, scanning electron microscope (SEM) (Hitachi S-2700, Japan) and transmission

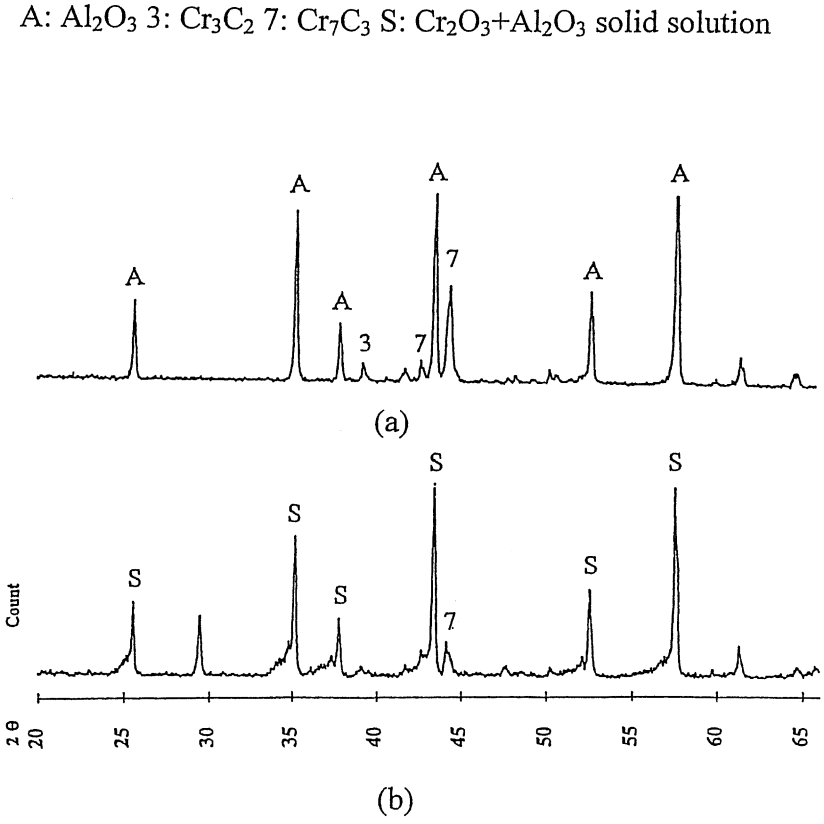

Fig. 1. X-ray diffraction patterns of 10 vol.% Cr_3C_2/Al_2O_3 composites: (a) as sintered (b) heat treated at 1200 °C 36 h in air.

electron microscope (TEM) (Jeol 3010, Japan). Phases in sintered samples were analyzed by X-ray diffractometer (Rigaku D/Max-IIB, Japan) using a Cu target and Ni filter at a speed of 4° /min from 20 to 80°. The residual stress was measured by a diffractometer (Siemens D-5000, Germany) following the $\sin^2\Psi$ method of Cohen et al.[16,17]

3. Results and discussion

3.1. Phases and microstructure

The X-ray diffraction (XRD) pattern of as sintered Cr_3C_2/Al_2O_3 composite is shown in Fig. 1(a). Results indicated that some Cr_3C_2 were oxidized, decarbonized and transformed into Cr_7C_3. The following reaction is favoured according to the thermodynamic calculations.[18]

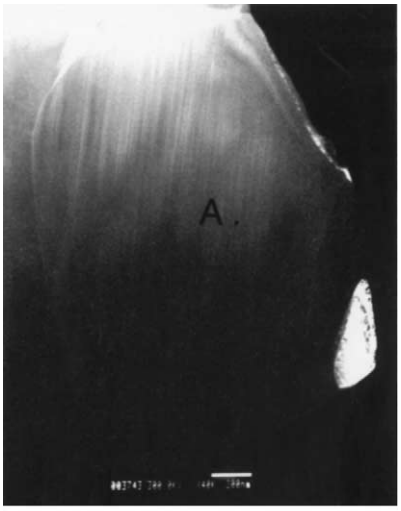

(a)

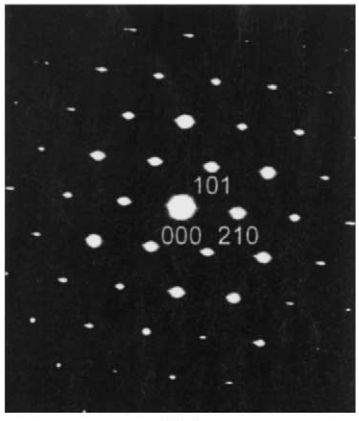

(b)

Fig. 2. Typical TEM micrographs of 10 vol.% Cr_3C_2/Al_2O_3 composite: (a) bright-field image; (b) SADP image of area A in (a).

$$Cr_3C_2(s) + (5/14)O_2(g) = (3/7)Cr_7C_3(s) + (5/7)CO(g) \quad (1)$$

Results of XRD analysis showed that most of the Cr_3C_2 and Cr_7C_3 disappeared after being heat treated at 1200 °C for 36 h in air [Fig. 1(b)]. In addition, the alumina peaks shift 0.1° toward smaller 2θ after heat treatment. Previous investigation by high temperature XRD analysis indicated that the possible oxidation and compositional change of Cr_3C_2 and Cr_7C_3 at 1200 °C in vacuum can be expressed by the following equations.[2,4,18]

$$2Cr_3C2(s) + (13/2)O_2(g) = 3Cr_2O_3(s) + 4CO(g) \quad (2)$$

$$2Cr_7C_3(s) + (27/2)O_2(g) = 7Cr_2O_3(s) + 6CO(g) \quad (3)$$

$$Cr_2O_3(s) + (3/2)O_2(g) = 2CrO_3(g) \quad (4)$$

Both Cr_2O_3 and Al_2O_3 have corundum structure and the ionic radius of Al^{+3} (0.68 Å) is only slightly smaller than that of Cr^{+3} (0.76 Å) ions. Therefore, the alumina peaks shifted after heat treatment possibly because the Cr_2O_3 reacted with Al_2O_3 to form a Al_2O_3–Cr_2O_3 solid solution. It was formerly suggested that the lattice parameters of the solid solution deviate slightly from Vegard's law[19] and the amount of change depends on the sintering kinetics and solubility of chromium oxide in alumina.[20] Similar results on the possible formation of solid solution have been previously reported.[2,21,22]

It was previously proposed that the Cr_2O_3 phase is not a stable phase at elevated temperatures in the ambient atmosphere and it continues to react with oxygen to form the CrO_3 gas phase as expressed by Eq. (4).[18,23] The CrO_3 gas can vaporize at elevated temperature, condense and precipitate on the sample surfaces as the temperature decreases.[2] Fig. 2(a) shows a typical TEM bright-field image of the oxidized chromium carbide in Cr_3C_2/Al_2O_3 composite. The selected area diffraction pattern of area A in Fig. 2(a) indicates the formation of orthorhombic Cr_7C_3 phase from Cr_3C_2 after sintering [Fig. 2(b)]. These observations are in good agreement with the results of X-ray analysis as discussed in Fig. 1(a).

The results of EDS analysis showing the surface oxidation layer and interior bulk of heat-treated Cr_3C_2/Al_2O_3 composite are displayed in Fig. 3(a) and (b), respectively. The results indicated that the Cr composition was reduced substantially after oxidation. This could be explained by the vaporization of CrO_3 gas as expressed by Eq. (4). A typical fractured surface of Cr_3C_2/Al_2O_3 composite after heat treatment is shown in Fig. 4(a). An oxidation layer of 5 μm in thickness was noticed after heat treatment. Some oxidation-induced micropores were observed near the surface layer as

shown in Fig. 4(b). The presence of pores was probably due to the CrO_3 diffusing outward through the Al_2O_3 matrix as discussed in Fig. 3.

3.2. Residual stresses of oxidation layer

3.2.1. Indentation method

The presence of residual stress could be due to the difference in thermal expansion coefficient between the surface oxidation layer and substrate material. Surface residual stresses were evaluated by an indentation method proposed by Marshall et al.[24–26] If a surface compressive residual stress of magnitude σ_R exists, then the stress intensity is given by:

$$K = \chi\left(P/C^{3/2}\right) - 2m\sigma_R(C/\pi)^{1/2} \quad (5)$$

The first term in Eq. (5) represents the indentation driving force, where P is the applied load, C is the crack dimension, and χ is the proportionality constant. The second term indicates the residual resistance force, and m is a dimensionless modification factor whose value is unity when free-surface effects and stress gradients are neglected. The crack remains in stable equilibrium during its growth if $K = K_c$ (fracture toughness) is satisfied. The general equilibrium equation may be written as follows :

$$\left(P/C^{3/2}\right)_{\sigma R} = \left(P/C^{3/2}\right)_0\left(1 + \left(2m\sigma_R C^{1/2}\right)/\left(\pi^{1/2}K_c\right)\right) \quad (6)$$

where $(P/C^{3/2})_0 = (K_c/\chi) = \text{constant}$, when the crack length is measured in a stress-free state. The surface residual stresses σ_R could be obtained from the plot of $(P/C^{3/2})_{\sigma R}$ versus $C^{1/2}$. The calculated surface compressive stress for as sintered and heat treated samples were 0 and −195 MPa, respectively as illustrated in Fig. 5.

3.2.2. X-ray diffraction method

In order to compare with the indentation method, the residual stress was also measured by a $\sin^2\psi$ method.[16,17] The stress is calculated from the variation in interplanar spacing within the crystal determined

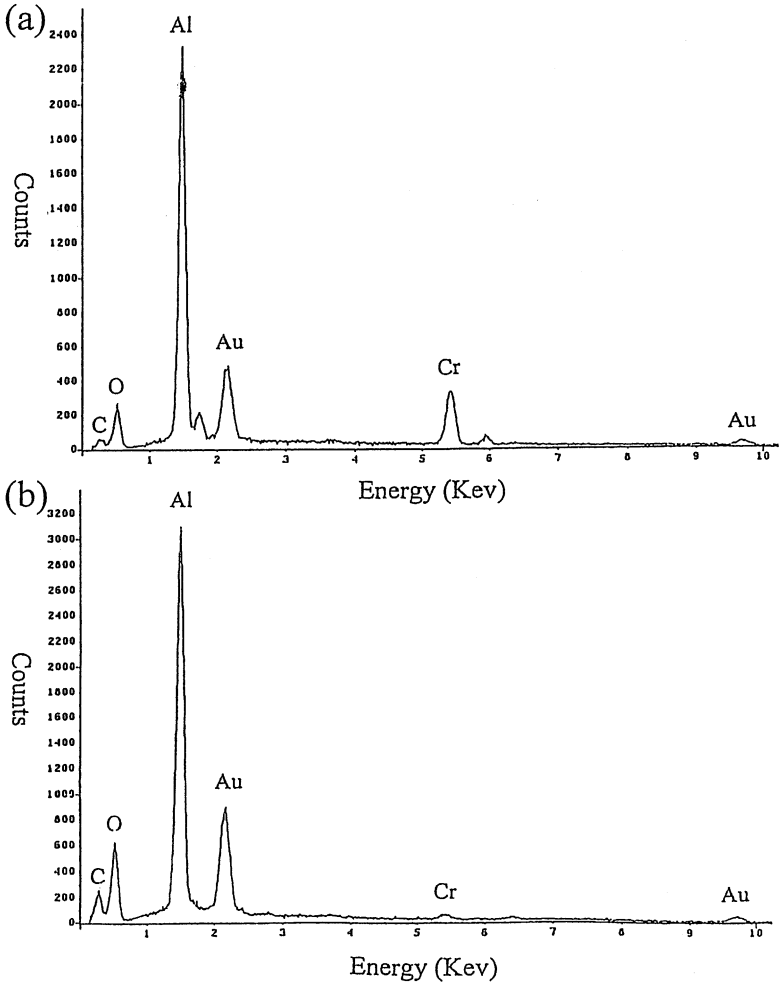

Fig. 3. EDS patterns of 10 vol.% Cr_3C_2/Al_2O_3 composites with unoxidized area (a) and oxidized surface (b).

from the X-ray diffraction. When a biaxial stress exists in the surface layer, the lattice strain is correlated to the stress by :

$$\varepsilon = (d_{\Phi\Psi} - d_0)/d_0$$

$$= [(1+\nu)/E]\sigma_\Phi \sin^2\Psi - (\nu/E)(\sigma_{11}+\sigma_{12}) \quad (7)$$

where d_0 is the unstressed lattice spacing, $d_{\Phi\psi}$ is the stressed lattice spacing, σ_Φ is the stress component along the direction Φ defined in the oxidation layer, Ψ is the tilt angle, σ_{11} and σ_{22} are the principal stress, E is the Young's modulus and ν is the Poisson's ratio. The E and ν were calculated as 360 GPa and 0.24, respectively

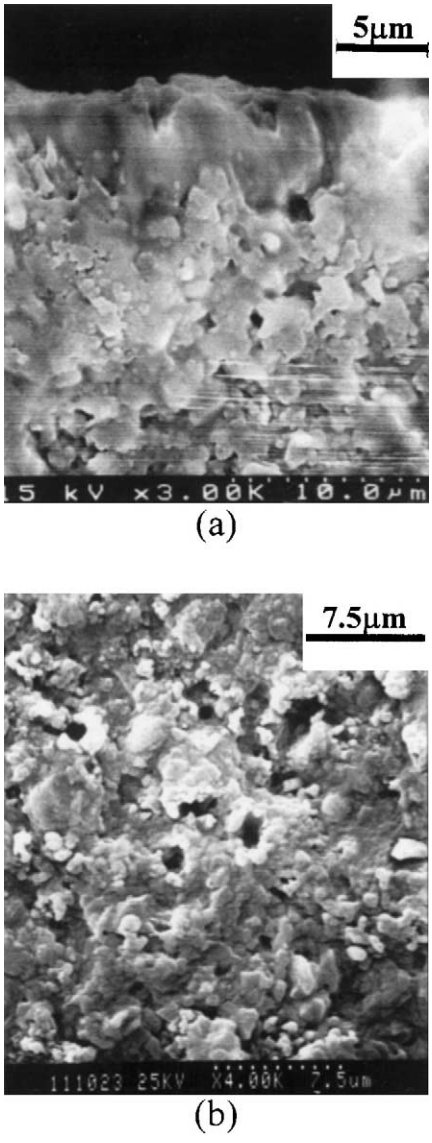

Fig. 4. SEM micrographs showing cross-section of oxidized layer (a) and surface with micropores (b) after oxidation of 10 vol.% Cr_3C_2/Al_2O_3 composite.

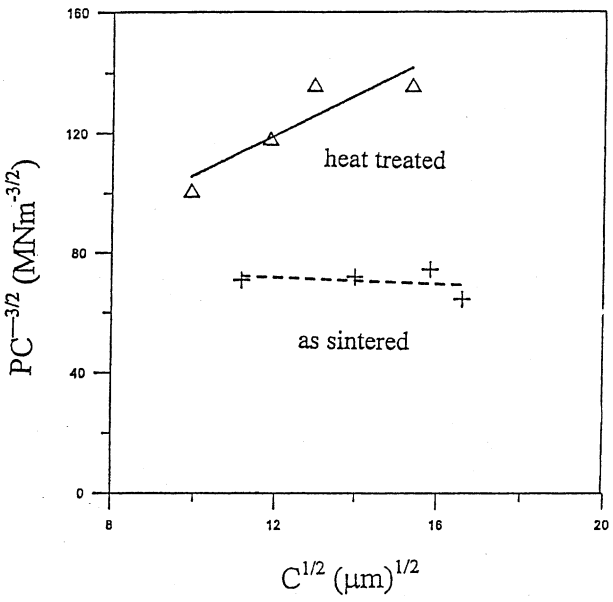

Fig. 5. Plots of ($P/C^{3/2}$) versus $C^{1/2}$ for as sintered and heat treated 10 vol.% Cr_3C_2/Al_2O_3 composites.

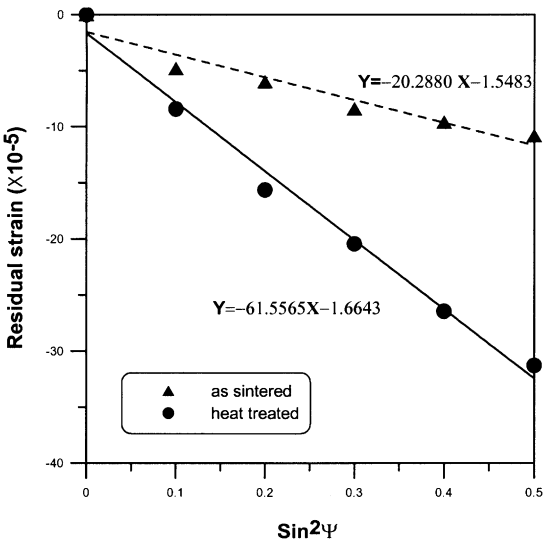

Fig. 6. Residual strains of as sintered and heat treated 10 vol.% Cr_3C_2/Al_2O_3 composites obtained from (416) reflection.

Table 1
Residual stresses of 10% Cr_3C_2/Al_2O_3 composite induced by oxidization in air at 1200 °C (36 h)

	Indentation method	X-ray measurement	Mismatch of TEC
As sintered (MPa)	0	−59	0
Heat treated (MPa)	−195	−179	−139

for 10% Cr_3C_2/Al_2O_3 composite. By virtue of the Bragg's condition for diffraction, stress can be calculated from Eq. (8).

$$\sigma = [E/(1+\nu)]\{\partial(\varepsilon)/\partial(\sin^2\Psi)\} \quad (8)$$

The residual strains of as sintered and heat treated Cr_3C_2/Al_2O_3 from the (416) reflections are shown in Fig. 6. A residual compressive stress of −59 MPa in the as-sintered specimens, and −179 MPa in the heat treated sampleswere therefore obtained from Eq. (8). These values were slightly different from those determined by indentation (Table 1). The stress retention observed in the as-sintered samples by the X-ray diffraction method may have been induced from sample machining, lapping and polishing. The difference in residual stress between the indentation and X-ray diffraction methods could also arise because the stress gradients over the prospective crack depth are neglected by the indentation method which assumed the modification factor m in Eq. (5) to be unity.

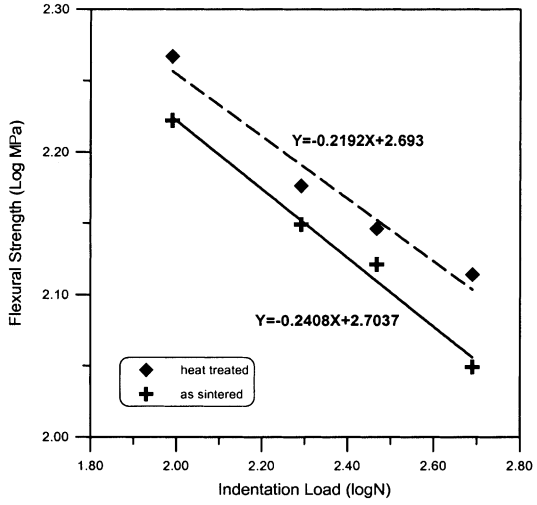

Fig. 7. Logarithmic plots of flexural strength versus indentation load for 10 vol.% Cr_3C_2/Al_2O_3 composites.

Fig. 9. TEM (Dark Field) micrograph illustrating a typical dislocation network from heat treated 10 vol.% Cr_3C_2/Al_2O_3 composite.

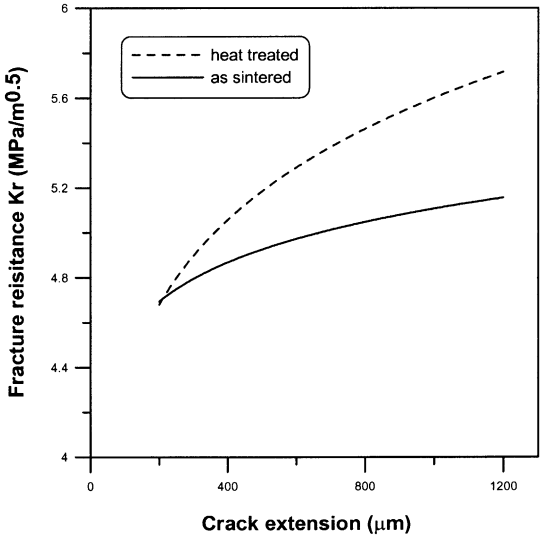

Fig. 8. R-curves of as sintered and heat treated 10 vol.% Cr_3C_2/Al_2O_3 composites.

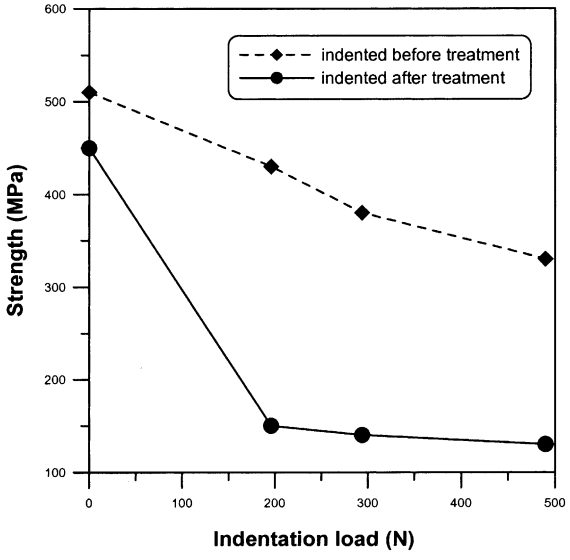

Fig. 10. Indentation fracture strengths for 10 vol.% Cr_3C_2/Al_2O_3 composites in both treated before and after indentation states.

3.2.3. Thermal mismatch induced residual stress

The stress caused by the difference in the thermal expansion coefficient between the surface oxidation layer and substrate material can be estimated from Eq. (9).[27]

$$\alpha = E(T - T_0)(\alpha_s - \alpha_m)\left(1 - 3j + 6j^2\right) \quad (9)$$

where T is the heat treatment temperature, T_0 is room temperature, α_s and α_m are the linear thermal expansion coefficients of the surface oxidation layer and matrix, respectively, E is the elastic modulus, and j is the ratio of the thickness of the surface oxidation layer to that of the matrix. The thermal expansion coefficients, α_s and $\alpha_{m,}$ were determined by a dilatometer (200–1200 °C) to be 8.43×10^{-6}/°C and 8.76×10^{-6}/°C, respectively. The residual stress due to thermal mismatch could therefore be calculated as −139 MPa from Eq. (9).

Table 1 summarized the residual compressive stresses determined by indentation method and X-ray diffraction as well as the theoretical value calculated from thermal mismatch. A net difference of −120 MPa between the as sintered and heated samples was observed by X-ray diffraction method. This value was slightly lower than the theoretical value calculated from TEC mismatch. This difference could be caused by the difficulty in determining the theoretical E values used in Eq. (9), due to the formation of the Cr_3C_2–Al_2O_3 solid solution.

3.3. R-curve behavior

Plots of the flexural strength as a function of indentation load for both as sintered and heat-treated specimens are shown in Fig. 7. The flexural strength decreased consistently with the applied indentation load. In addition, the strength of heat-treated samples was invariably higher than that of as sintered Cr_3C_2/Al_2O_3 composite. The R-curve plots derived from the results of Fig. 7 by assuming that the fracture toughness K_R is related to the crack length by a power-law relation as suggested by Krause[28] are shown in Fig. 8. The results revealed that R-curve behavior was most pronounced in heat-treated specimens with better fracture resistance than that of as sintered samples. Fig. 9 shows the typical TEM micrograph illustrating a dislocation network from heat treated Cr_3C_2/Al_2O_3 composite. Obviously, it resulted in a significant increase in the amount of dislocation density. This TEM microstructure provides additional evidence for better fracture resistance.

Table 2
Summary of 10% Cr_3C_2/Al_2O_3 composite crack healing observation

Indentation load (N)	Crack length (μm)	
	Untreated	Oxidization in air at 1200 °C (36 h)
196	216	105
294	274	134
490	402	202

It was formerly discussed that the residual stresses could have significant influence on the mechanical properties of ceramics.[7–10] A surface-compression-strengthened material can be considered to be toughened because the resistance to fracture from a surface crack is enhanced by the presence of surface compression.[29] Tandon and Green have shown that samples with residual compressive stress profiles below the surface could exhibit a rising R-curve behavior.[29] Similar effects of macroscopic residual stress on stress intensities of edge cracks and R-curves in three-layer composites for short cracks were previously discussed by Lakshminarayanan et al.[10]

3.4. Crack healing

The indentation fracture strengths of the 10 vol.% Cr_3C_2/Al_2O_3 composites respectively both treated before and after indentation states are shown in Fig. 10. Samples indented before treatment did not exhibit an appreciable decrease in strength. Comparing the crack length in untreated and heat treated samples as shown in Table 2, it is found that the crack length of treated samples has been almost halved. This observation can be attributed to crack healing. which could contribute partially to crack resistance. The presence of glassy phase could heal the propagating cracks and lower the stress-intensity factor at the crack tips. Similar observations were formerly discussed for SiC and Si_3N_4 composites.[30–32]

4. Conclusions

(1) A reaction layer consisting of Al_2O_3 and Cr_2O_3–Al_2O_3 solid solution with mismatch of thermal expansion coefficient gives rise to a compressive residual surface stress −179 MPa as detected by X-ray diffraction. (2) The established stress profile is an effective method for improving room temperature crack resistance at short crack lengths. Macroscopic surface compressive residual stress plays the primary role in crack resistance for Cr_3C_2/Al_2O_3 composites oxidation treatment.

Acknowledgements

The authors would like to thank the National Science Council, Republic of China, for its support under Grant No. NSC 87-2216-E006-041.

References

1. Fu, C. T., Wu, J. M. and Li, A. K., Microstructure and mechanical proterties of Cr_3C_2 particulate reinforced Al_2O_3 matrix composites. *J. Mater. Sci*., 1994, **29**, 2671–2677.
2. Fu, C. T., Li, A. K. and Wu, J. M., Effects of oxidation of Cr_3C_2 particle reinfroced Cr_3C_2 matrix composites on microstructure and mechanical structure properties. *J. Mater. Sci*., 1993, **28**, 6285–6294.
3. Fu, C. T., Li, A. K. and Wu, J. M., Effects of post-sinter hot isostatic pressing processes on microstructures and mechanical properties of Al_2O_3- Cr_3C_2 composites. *Br. Ceram. Trans*, 1994, **93**, 178–183.
4. Lii, D. F., Huang, J. L., Twu, K. C. and Li, A. K., Investigation of Al_2O_3/ Cr_3C_2 composites prepared by pressureless sintering (part 1). *J. Ceram. Soc. Jpn*., 1996, **104**, 796–801.
5. Huang, J. L., Twu, K. C., Lii, D. F. and Li, A. K., Investigation of Al_2O_3/ Cr_3C_2 composites prepared by pressureless sintering (part 2). *Mater. Chem. Phys*., 1997, **51**, 211–215.
6. Huang, J. L., Huang, J. J., Jeng, C. A. and Li, A. K., Investigation of Al_2O_3/ Cr_3C_2 composites prepared by pressureless sintering (part 3). *Ceram. Int*., 1999, **25**, 141–144.
7. Duke, D. A., Megles, J. E., MacDowell, J. E. and Bopp, H. E., Strengthening glass-ceramics by application of compressive glazes. *J. Am. Ceram. Soc*., 1968, **51**, 98–102.
8. Virkar, A. V., Huang, J. L. and Cutler, R. A., Strengthening of oxide ceramics by tranformation-toughened stresses. *J. Am. Ceram. Soc*., 1987, **70**, 164–170.
9. Green, D. J., A Technique for introducing surface compression into zirconia ceramics. *J. Am. Ceram. Soc*., 1983, **66**, C178–C179.
10. Lakshminarayanan, R., Shetty, D. K. and Cutler, R. A., Toughening of layered ceramic composites with residual surface compression. *J. Am. Ceram. Soc*., 1996, **79**, 79–87.
11. Tandan, R. and Green, D. J., Surface stress effects on indentation fracture sequences. *J. Am. Ceram. Soc*., 1990, **73**, 2619–2627.
12. Becher, P. F., Strength rentention in SiC ceramics after long-term oxidation. *J. Am. Ceram. Soc*., 1983, **66**, C120–C121.
13. Yoshimura, M., Ohji, T. and Niihara, K., Oxidation-induced toughening and strengthening of Y_2O_3/SiC nanocomposites. *J. Am. Ceram. Soc*., 1997, **80**, 797–799.
14. Tojek, K. K. and Green, D. J., Effect of residual stress on the strength distribution of brittle materials. *J. Am. Ceram. Soc*., 1989, **72**, 1885–1890.
15. Damani, R. J. and Lutz, E. H., Microstructure, strength and fracture characteristics of a free-standing plasma-sprayed alumina. *J. Eur. Ceram. Soc*., 1997, **17**, 1351–1359.
16. Cohen, J. B., Dolle, H. and James, M. R., *Stress Analysis from Powder Diffraction Patterns*. NBS Special Publication 567, 1980, pp. 453–477.
17. Noyan, I. C. and Cohen, J. B., *Residual Stress*. Springer Verlag, New York, 1987.
18. Lii, D. F., Huang, J. L., Huang, J. J. and Lu, H. H., The interfacial reaction in Cr_3C_2/Al_2O_3 composites. *J. Mater. Res*., 1999, **14**, 817–823.
19. Rossi, L. R. and Lawrence, W. G., Elastic properties of oxide solid solutions: the system Al_2O_3–Cr_2O_3. *J. Am. Ceram. Soc*., 1971, **53**, 604–608.
20. Han, H. C., Soon, D. Y. and Brum, M. K., Migration of grain boundaries in alumina induced by chromia addition. *Acta Metall. Mater*., 1995, **43**, 977.
21. Watanabe, M., Hirayama, T., Yoshinaka, M., Horita, K. and Yamaguchi, O., Formation of continuous series of solid solutions from powders prepared by hydrazine method: the system Al_2O_3–Cr_2O_3. *Mater. Res. Bull*, 1996, **31**, 861.
22. Li, C. L., Riu, D. H., Sekino, T. and Nihara, K., Fabrication and mechanical properties of solid solution with low addition of Cr_2O_3. *Key Engineering Materials*, 1999, **161–163**, 161–164.
23. Granam, H. C. and Davis, H. H., Oxidation/vaporization kinectics of Cr_2O_3. *J. Am. Ceram. Soc*., 1971, **54**, 89–93.
24. Marshall, D. B. and Lawn, B. R., An indentation technique for measuring strsses in tempered glass surfaces. *J. Am. Ceram. Soc*., 1977, **60**, 86–87.
25. Lawn, B. R. and Fuller, E. R. Jr., Measurement of thin-layer surface stresses by indentation fracture. *J. Mater. Sci*., 1984, **19**, 4061–4067.
26. Gruninger, M. F., Lawn, B. R., Farabaugh, E. N. and Wachtman, J. B. Jr., Measurement of residual stresses in coating on brittle subsrates by indentation. *J. Am. Ceram. Soc*., 1987, **70**, 344–348.
27. Kingery, W. D., Bowen, H. K. and Uhlmann, D. R., *Introduction to Ceramics*, 2nd edn. Wiley, New York, 1976.
28. Krause, R. F. Jr., Rising fracture toughness from the bending strength of indented alumina beams. *J. Am. Ceram. Soc*., 1988, **71**, 338–343.
29. Tandan, R. and Green, D. J., Crack stability and t-curve due to macroscopic residual compressive stress profiles. *J. Am. Ceram. Soc*., 1991, **74**, 1981–1986.
30. Lange, F. F., Healing of surface cracks in SiC by oxidation. *J. Am. Ceram. Soc*., 1970, **53**, 290.
31. Zhang, Y. H., Edwards, L. and Plumbridge, W. J., Crack healing in a silicon nitride ceramics. *J. Am. Ceram. Soc*., 1998, **81**, 1861–1868.
32. Chiu, C. C., Influence of surface oxidation on thermal shock resistance and flexural strength of SiC/Cr_3C_2 composites. *J. Mater. Sci*., 1994, **29**, 2078–2082.